Article

Immunity

Inflammasome Activation Triggers Blood Clotting and Host Death through Pyroptosis

Graphical Abstract

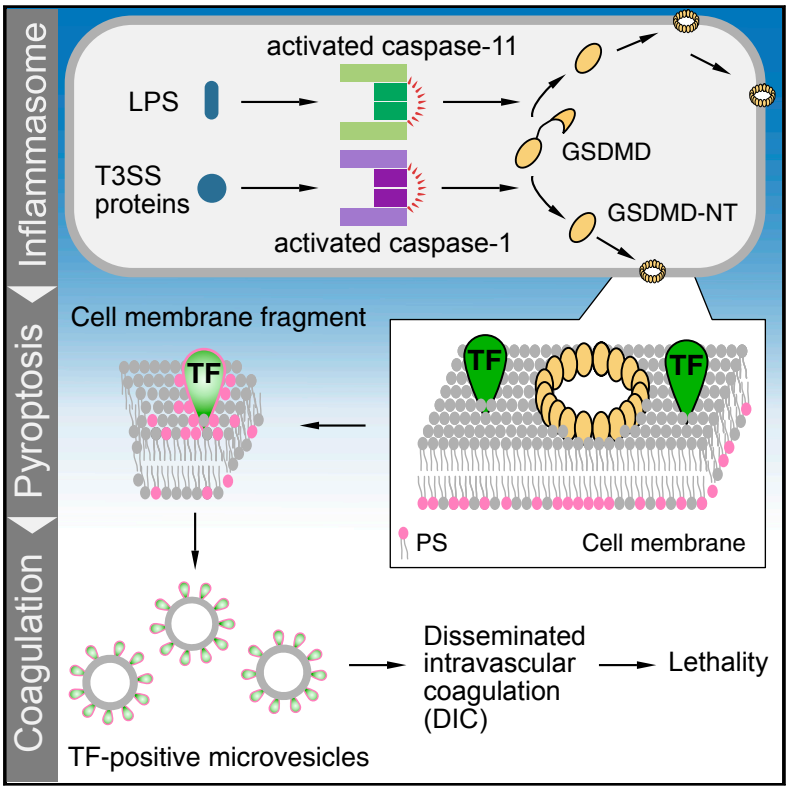

Authors

Congqing Wu, Wei Lu, Yan Zhang, ..., Nigel Mackman, Yinan Wei, Zhenyu Li

Correspondence

yinan.wei@uky.edu (Y.W.), zhenyuli08@uky.edu (Z.L.)

In Brief

Overactivation of inflammasome leads to death of the host. Wu and colleagues demonstrate that activation of coagulation is responsible for inflammasome activation-induced death.

Highlights

- Canonical or noncanonical inflammasome activation leads to blood clotting
- Inflammasome activation induces blood clotting through pyroptosis
- Tissue factor released from pyroptotic macrophages drives blood blotting
- Interfering tissue factor prevents pyroptosis-induced lethality

Wu et al., 2019, Immunity *50*, 1401–1411
June 18, 2019
https://doi.org/10.1016/j.immuni.2019.04.003

CellPress

Immunity
Article

Inflammasome Activation Triggers Blood Clotting and Host Death through Pyroptosis

Congqing Wu,[1] Wei Lu,[2] Yan Zhang,[1] Guoying Zhang,[1] Xuyan Shi,[3] Yohei Hisada,[4] Steven P. Grover,[4] Xinyi Zhang,[2] Lan Li,[2] Binggang Xiang,[1] Jumei Shi,[5] Xiang-An Li,[6] Alan Daugherty,[1,6] Susan S. Smyth,[1,7] Daniel Kirchhofer,[8] Toshihiko Shiroishi,[9] Feng Shao,[3] Nigel Mackman,[4] Yinan Wei,[2,*] and Zhenyu Li[1,10,*]

[1]Saha Cardiovascular Research Center, College of Medicine, University of Kentucky, Lexington, KY, USA
[2]Department of Chemistry, College of Arts and Sciences, University of Kentucky, Lexington, KY, USA
[3]National Institute of Biological Sciences, Beijing, China
[4]Division of Hematology and Oncology, Department of Medicine, McAllister Heart Institute, University of North Carolina at Chapel Hill, Chapel Hill, NC, USA
[5]Department of Hematology, Shanghai Tenth People's Hospital, Tongji University Cancer Center, Tongji University School of Medicine, Shanghai, China
[6]Department of Physiology, College of Medicine, University of Kentucky, Lexington, KY, USA
[7]Veterans Affairs Medical Center, Lexington, KY, USA
[8]Department of Early Discovery Biochemistry, Genentech, Inc., South San Francisco, CA, USA
[9]Mammalian Genetics Laboratory, Genetic Strains Research Center, National Institute of Genetics, Mishima, Shizuoka, Japan
[10]Lead Contact
*Correspondence: yinan.wei@uky.edu (Y.W.), zhenyuli08@uky.edu (Z.L.)
https://doi.org/10.1016/j.immuni.2019.04.003

SUMMARY

Inflammasome activation and subsequent pyroptosis are critical defense mechanisms against microbes. However, overactivation of inflammasome leads to death of the host. Although recent studies have uncovered the mechanism of pyroptosis following inflammasome activation, how pyroptotic cell death drives pathogenesis, eventually leading to death of the host, is unknown. Here, we identified inflammasome activation as a trigger for blood clotting through pyroptosis. We have shown that canonical inflammasome activation by the conserved type III secretion system (T3SS) rod proteins from Gram-negative bacteria or noncanonical inflammasome activation by lipopolysaccharide (LPS) induced systemic blood clotting and massive thrombosis in tissues. Following inflammasome activation, pyroptotic macrophages released tissue factor (TF), an essential initiator of coagulation cascades. Genetic or pharmacological inhibition of TF abolishes inflammasome-mediated blood clotting and protects against death. Our data reveal that blood clotting is the major cause of host death following inflammasome activation and demonstrate that inflammasome bridges inflammation with thrombosis.

INTRODUCTION

Inflammasomes are intracellular sensory complexes that detect invading bacterial pathogens in the cytosol. Activation of the inflammatory caspases, including caspase-1 and caspase-11 (caspase-4 and -5 in human), by microbial products leads to interleukin (IL)-1β and IL-18 maturation and release and a lytic cell death termed pyroptosis (Fink and Cookson, 2006; Lamkanfi and Dixit, 2014; Schroder and Tschopp, 2010). Caspase-1 is activated by Gram-negative bacterial flagellin and type III secretion system (T3SS) apparatus proteins through NLRC4 inflammasome (Miao et al., 2010; Zhao et al., 2011). Caspase-11 is activated by cytoplasmic lipopolysaccharide (LPS) through noncanonical inflammasome pathway (Hagar et al., 2013; Kayagaki et al., 2013; Shi et al., 2014; Vanaja et al., 2016). Activated caspase-1 and -11 cleave gasdermin D (GSDMD), triggering the formation of pores in plasma membrane (Aglietti et al., 2016; Ding et al., 2016; Liu et al., 2016; Ruan et al., 2018; Sborgi et al., 2016). The pores formed by GSDMD have been shown to facilitate IL-1β release (Evavold et al., 2018; He et al., 2015; Monteleone et al., 2018). Formation of pores in cell membranes also drives pyroptosis, a form of osmotic cell lysis accompanied by ruptured cell membranes (He et al., 2015; Kayagaki et al., 2015; Shi et al., 2015). Inflammasome activation and subsequent pyroptosis support host defense against bacterial pathogens; however, their hyperactivity has devastating consequences, such as multiple organ dysfunction and lethality (Aziz et al., 2013; Zhao et al., 2016). T3SS rod proteins, flagellin, and LPS have been shown to trigger macrophage pyroptosis and death of the host (Kayagaki et al., 2013; Zhao et al., 2016). The underlying mechanisms of host death following pyroptotic cell death of macrophages have not been defined.

Blood coagulation is essential for hemostasis to stop bleeding after injury. In contrast, disseminated intravascular coagulation (DIC) is a pathologic state of systemic activation of blood coagulation. DIC often accompanies sepsis and results in microvessel occlusion, organ dysfunction, and death (Gando et al., 2016; Levi and Ten Cate, 1999). Mortality rate doubles in septic patients with DIC compared to patients without DIC (Fujishima et al., 2014; Gando et al., 2013; Rangel-Frausto et al., 1995; Venugopal, 2014). As the primary initiator of coagulation, tissue factor (TF) plays an essential role in initiating DIC in systemic

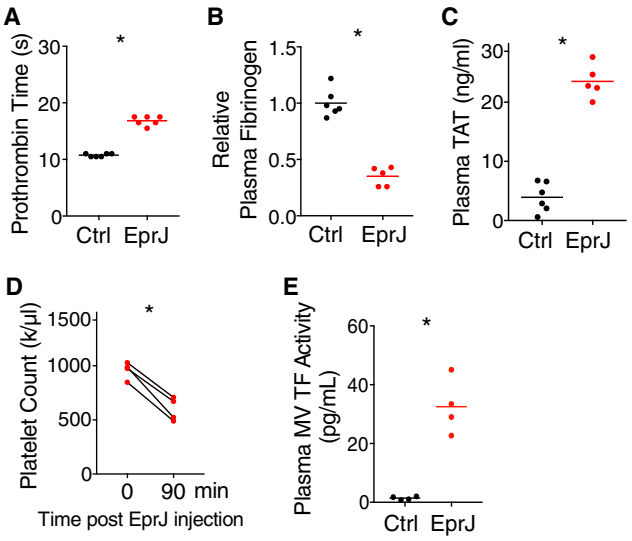

Figure 1. Administration of EprJ *In Vivo* Induces Systemic Coagulation

(A–E) Mice (C57BL/6J) were injected intravenously with PBS (Ctrl) or EprJ (300 ng LFn-EprJ plus 3 μg PA per mouse). Blood was collected 90 min after PBS or EprJ injection. Prothrombin time (A), plasma fibrinogen concentrations (B), plasma TAT concentrations (C), total platelet count before and after EprJ injection (D), and TF activity in plasma microvesicles (MVs) (E) were measured. Solid circles represent individual mice; crossbars represent group mean. n = 4–6 for all experimental groups. *$p < 0.01$ (Student's t test; unpaired for A–C and E; paired for D).

See also Figure S1.

inflammatory disorders, including sepsis (Franco et al., 2000; Gando et al., 2016; Pawlinski et al., 2004, 2010; Taylor et al., 1991). The mechanisms for blood coagulation induced by bacterial infection are often attributed to host inflammatory response to bacterial virulence factors (Gando et al., 2016), yet the molecular events linking bacterial infection to TF release that triggers coagulation cascade are unknown.

Here, we show that inflammasome activation leads to TF release in the form of microvesicles (MVs), which triggers systemic coagulation and lethality. TF release following inflammasome activation depends on pyroptosis. Deficiency of GSDMD, but not the receptor of IL-1β or IL-18, abolishes the activation of coagulation induced by *E. coli* T3SS rod protein EprJ. Pharmacological or genetic inhibition of TF prevented EprJ-induced DIC and lethality. Our findings identify a molecular mechanism of DIC in sepsis and reveal how inflammasome activation and pyroptosis lead to death of the host.

RESULTS

Inflammasome Activation by Bacterial Rod Protein EprJ Causes Systemic Coagulation

To identify the mechanism by which inflammasome activation leads to death of the host, we injected C57BL/6J mice with the *E. coli* T3SS inner rod protein EprJ. EprJ was fused to the cytosolic translocation domain of anthrax lethal factor (LFn) to enable efficient cytosolic delivery. LFn binds to anthrax protein protective agent (PA), which delivers the LFn-EprJ fusion protein into the cytoplasma through receptor-mediated endocytosis (Milne et al., 1995; Zhao et al., 2011). We found that purified EprJ (LFn-EprJ plus PA) induced robust caspase-1 activation and pyroptosis (Figures S1A and S1B) in mouse primary bone-marrow-derived macrophages (BMDMs). Intravenous injection of EprJ caused hemolysis in C57BL/6J mice (Figure S1C). Red blood cells did not rupture when incubated *ex vivo* with EprJ (Figure S1D), eliminating a direct effect of EprJ on red blood cells leading to hemolysis.

As hemolysis could be a consequence of DIC (Effenberger-Neidnicht and Hartmann, 2018), we investigated whether EprJ was capable of initiating blood coagulation. We first performed a series of assays commonly used for DIC diagnosis (Wada et al., 2014). Patients with DIC often have prolonged prothrombin time (PT) due to consumption of coagulation factors (Angus and van der Poll, 2013; Gando et al., 2016; Levi and Ten Cate, 1999; Wada et al., 2014). Indeed, PT was prolonged significantly in C57BL/6J mice challenged with EprJ, as demonstrated by a standard PT assay (Figure 1A). PA alone had no effects (Figure S1E). During DIC, fibrinogen is cleaved into fibrin by thrombin (Wada et al., 2014), resulting in a decrease in plasma fibrinogen concentrations. As expected, plasma fibrinogen concentrations were reduced in C57BL/6J mice receiving EprJ (Figure 1B). EprJ elevated plasma thrombin-antithrombin (TAT) concentrations, indicating heightened conversion of prothrombin to thrombin (Figure 1C). EprJ also caused thrombocytopenia in C57BL/6J mice (Figure 1D), another clinical feature consistent with DIC. TF plays a key role in triggering blood clotting in sepsis (Bach et al., 1981; Levi et al., 1994; Morrissey et al., 1987; Pawlinski et al., 2004; Taylor et al., 1991), and TF activity in plasma MVs was increased in mice challenged with EprJ (Figure 1E).

In DIC, systemic activation of the clotting cascade leads to fibrin deposition and formation of microthrombi throughout vasculature (Levi and Ten Cate, 1999). Indeed, administration of EprJ in C57BL/6J mice induced thrombus formation, as evidenced by occlusion in cremaster vasculature, platelet accumulation, and fibrin deposition detected by intravital microscopy (Figure 2A; Video S1). The mice were injected with washed platelets isolated from the GFP-expressing mice C57BL/6-Tg(CAGEGFP)1Osb/J and Alexa Fluor 568-labled anti-fibrin antibody (59D8), which is a monoclonal antibody specifically recognizing mouse fibrin (Hui et al., 1983; Ivanciu et al., 2011; Neyman et al., 2008; Weiler-Guettler et al., 1998). Fibrin deposition was also detected in liver by immunostaining (Figure 2B). Immunoblot analysis revealed significant accumulation of fibrin in liver and spleen in mice challenged with EprJ (Figure 2C). Together, these data demonstrate that EprJ induces systemic coagulation in mice.

Coagulation Activation Induced by Rod Proteins Requires Caspase-1

Next, we examined the role of inflammasome in EprJ-induced coagulation with caspase-1-deficient mice. As widely used caspase-1-deficient mice lack both caspase-1 and caspase-11 (Kayagaki et al., 2011), they are referred to as *Casp1/11*$^{-/-}$ hereafter. Coagulation activation triggered by EprJ was diminished in *Casp1/11*$^{-/-}$ mice, as shown by loss of fibrin deposition in tissues (Figures 2A–2C; Video S1). EprJ-induced prolongation of PT (Figure 2D), reduction in plasma fibrinogen concentrations (Figure 2E), and increase in plasma TAT concentrations

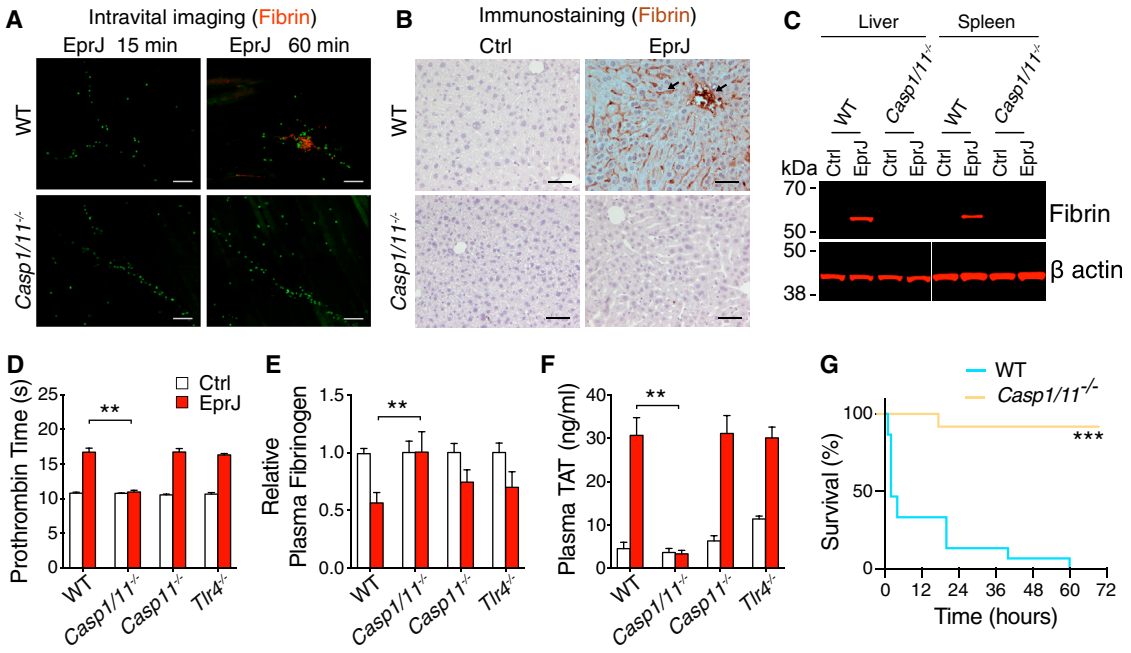

Figure 2. Caspase-1 Is Required for EprJ-Induced Blood Coagulation and Lethality

(A) C57BL/6J mice (wild-type [WT]) or Casp1/11-deficient mice were injected intravenously with washed platelets isolated from the C57BL/6-Tg(CAG-EGFP) 1Osb/J mice (GFP) and an Alexa Fluor 568-labled (red) anti-fibrin monoclonal antibody (59D8), followed by intravenous injection of EprJ. Thrombus formation in cremaster vasculatures was monitored using an intravital microscopy. Images were acquired at the same location, 15 min and 60 min after EprJ injection. Scale bars denote 50 μm. Data are representative of 3 independent experiments (biological replicates).

(B) C57BL/6J mice (WT) or Casp1/11-deficient mice were injected intravenously with EprJ. After 90 min, mice were euthanized and perfused with PBS and then perfusion fixed with 10% formalin under physiological pressure for 45 min. Liver sections were immunostained with the anti-fibrin monoclonal antibody (59D8). Wild-type mice, but not *Casp1/11*$^{-/-}$ mice, showed fibrin deposition in liver (arrows). Scale bars denote 50 μm. Data are representative of 3 independent experiments (biological replicates).

(C) C57BL/6J mice (WT) or Casp1/11-deficient mice were injected intravenously with EprJ. After 90 min, mice were euthanized, and tissues were isolated. Fibrin in the tissue lysates was detected by immunoblot with the anti-fibrin monoclonal antibody (59D8). Data are representative of 3 independent experiments (biological replicates).

(D–F) C57BL/6J mice (WT), Casp1/11-deficient mice, Casp11-deficient mice, and TLR4-deficient mice were injected intravenously with PBS or EprJ. Blood was collected 90 min after PBS or EprJ injection. Prothrombin time (D), plasma fibrinogen concentrations (E), and plasma TAT concentrations (F) were measured. Error bars denote SEM; n = 4–6 for all experimental groups. **p < 0.01 (two-way ANOVA with Holm-Sidak multiple comparisons).

(G) C57BL/6J mice (WT) or Casp1/11-deficient mice were injected intravenously with a lethal dose of EprJ. Kaplan-Meier survival plots for mice challenged with EprJ are shown. n = 12–15. ***p < 0.01 versus WT (log rank test [Mantel-Cox]).

See also Figure S1.

(Figure 2F) were diminished in *Casp1/11*$^{-/-}$ mice. *Casp1/11*$^{-/-}$ mice were protected from EprJ-induced lethality (Figure 2G). To clarify the role of caspase-1, we determined whether caspase-11 was involved in EprJ-induced coagulation using *Casp11*$^{-/-}$ mice. Caspase-11 deficiency had no effect on PT, plasma fibrinogen concentrations, or plasma TAT concentrations in mice challenged with EprJ (Figures 2D–2F). In addition, EprJ elicited coagulation in *Tlr4*$^{-/-}$ mice (Figures 2D–2F). These findings indicate that blood coagulation elicited by EprJ is dependent on caspase-1, the key protease of inflammasome activity. To verify that caspase-1 is responsible for EprJ-elicited coagulation, we used newly developed "clean" *Casp1*$^{-/-}$ mice (Kayagaki et al., 2015). As expected, EprJ-induced coagulation was abolished in *Casp1*$^{-/-}$ mice (Figures S1F and S1G).

Inflammasome Activation Drives Coagulation and Lethality through Pyroptosis

Inflammasome activation leads to IL-1β and IL-18 maturation and release (Lamkanfi and Dixit, 2014; Schroder and Tschopp, 2010) and rapid production of inflammatory lipid mediators (von Moltke et al., 2012). EprJ-induced coagulation in *Il1r*$^{-/-}$ and *Il18r*$^{-/-}$ mice lacking the receptors of IL-1β and IL-18, respectively, to a similar extent as in wild-type mice (Figures S2A and S2B). These data support that coagulation following inflammasome activation is independent of IL-1β and IL-18.

Eicosanoids synthesized by cyclo-oxygenases have been shown to be critical mediators of inflammation and vascular fluid loss following inflammasome activation by flagellin (von Moltke et al., 2012). To determine whether cyclo-oxygenase (COX1 and COX2)-generated lipid mediators were involved in inflammasome-induced coagulation, mice were pretreated with the COX inhibitor aspirin prior to exposure to EprJ. Arachidonic acid-induced platelet aggregation requires COX-dependent TXA2 synthesis (Parise et al., 1984). As expected, arachidonic acid failed to elicit platelet aggregation in the mice pretreated with aspirin (Figure S2C). However, aspirin had no effect on PT prolongation or elevated plasma TAT concentrations (Figures S2D and S2E), effectively ruling

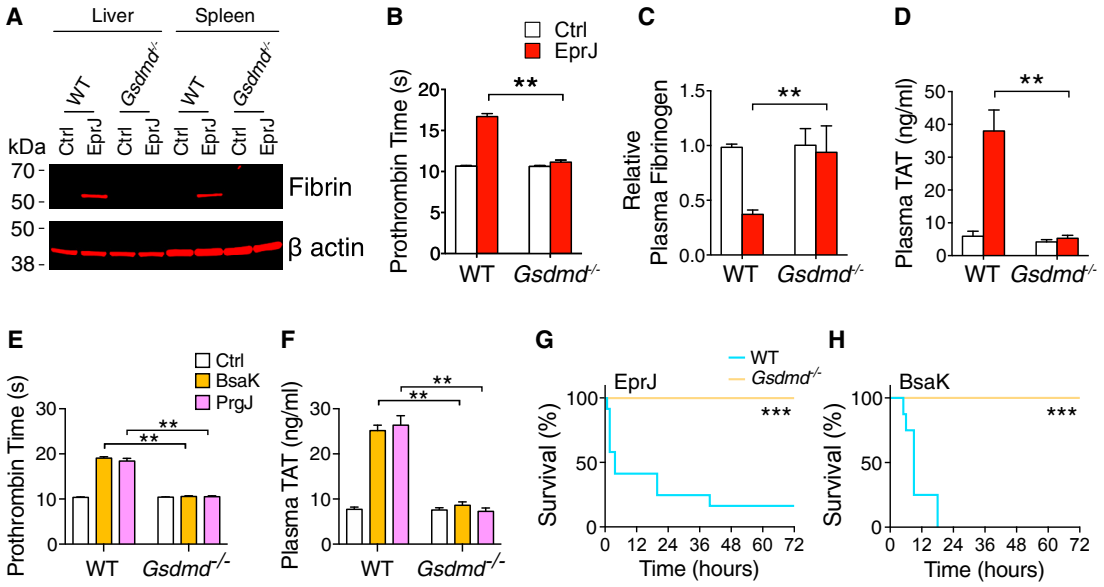

Figure 3. GSDMD-Dependent Pyroptosis Is Essential to Inflammasome-Driven Coagulation and Lethality

(A) C57BL/6J (WT) or GSDMD-deficient mice were injected intravenously with EprJ. After 90 min, mice were euthanized, and tissues were isolated. Fibrin in the tissue lysates was detected by immunoblot with the anti-fibrin monoclonal antibody (59D8). Data are representative of 3 independent experiments (biological replicates).

(B–D) C57BL/6J mice (WT) or GSDMD-deficient mice were injected intravenously with PBS (Ctrl) or EprJ. Blood was collected 90 min after PBS or EprJ injection. Prothrombin time (B), plasma fibrinogen concentrations (C), and plasma TAT concentrations (D) were measured. Error bars denote SEM; n = 4–6 for all experimental groups. **p < 0.01 (two-way ANOVA with Holm-Sidak multiple comparisons).

(E and F) C57BL/6J mice (WT) or GSDMD-deficient mice were injected intravenously with PBS (Ctrl) or BsaK or PrgJ. Blood was collected 90 min after the injection. Prothrombin time (E) and plasma TAT concentrations (F) were measured. Error bars denote SEM; n = 5 for all experimental groups. **p < 0.01 (two-way ANOVA with Holm-Sidak multiple comparisons).

(G and H) C57BL/6J mice (WT) or GSDMD-deficient mice were injected intravenously with a lethal dose of EprJ (G) or BsaK (H). Kaplan-Meier survival plots for mice challenged with EprJ are shown. n = 8–12. ***p < 0.01 versus WT (log rank test [Mantel-Cox]).

See also Figures S2, S3, and S4.

out a role for COX-mediated pathways in EprJ-induced coagulation.

Recent studies show that caspase-1 cleaves GSDMD and triggers pyroptosis—a form of programmed cell death with similar morphology to necrosis (Kayagaki et al., 2015; Shi et al., 2015). Consistent with these *in vitro* findings, EprJ injection caused peripheral monocyte depletion (Figure S3A), macrophage depletion, and cell death (Figures S3B and S3C). GSDMD deficiency protects against macrophage cell death and lethal endotoxemia (Kayagaki et al., 2015; Shi et al., 2015). We tested the hypothesis that GSDMD-dependent pyroptosis drives inflammasome-induced coagulation and lethality using *Gsdmd*$^{-/-}$ mice (Fujii et al., 2008). Indeed, fibrin deposition induced by EprJ was abolished by GSDMD deficiency (Figure 3A). EprJ-induced prolongation of PT (Figure 3B), reduction in plasma fibrinogen concentrations (Figure 3C), and increase in plasma TAT concentrations (Figure 3D) were also diminished in *Gsdmd*$^{-/-}$ mice. GSDMD deficiency also prevented systemic activation of coagulation induced by *E. coli* infection (Figures S4A and S4B). To determine whether inflammasome activation and subsequent pyroptosis are a common underlying mechanism for triggering coagulation, we examined the effects of rod proteins from other bacterial strains, such as *Burkholderia* BsaK and *Salmonella* PrgJ, on coagulation. Injection of BsaK and PrgJ proteins into C57BL/6 mice both elicited severe coagulation (Figures 3E and 3F), which was not observed in the *Gsdmd*$^{-/-}$ mice. Furthermore, GSDMD deficiency protected against EprJ- or BsaK-induced lethality (Figures 3G and 3H).

Monocytes and Macrophages Are Major Contributors to Inflammasome-Activation-Induced Coagulation and Lethality

Monocytes and macrophages are essential in inflammasome detection of bacterial infection (Lamkanfi and Dixit, 2014; Latz et al., 2013; Schroder and Tschopp, 2010). To determine the contribution of monocytes and macrophages to EprJ-induced coagulation, we depleted these cells by administration of commonly used clodronate-containing liposomes. Consistent with our previous report (Xiang et al., 2013), clodronate administration reduced blood monocytes by 90% within 24 h. Pre-depletion of monocytes and macrophages significantly attenuated EprJ-induced coagulation, as measured by PT, plasma fibrinogen, and TAT concentrations (Figures 4A–4C), supporting a central role of monocytes and/or macrophages in EprJ-induced coagulation. Furthermore, their importance in inflammasome-induced lethality was established by the fact that depletion of monocytes and macrophages using clodronate-containing liposomes significantly improved survival in mice challenged with a lethal dose of EprJ (Figure 4D).

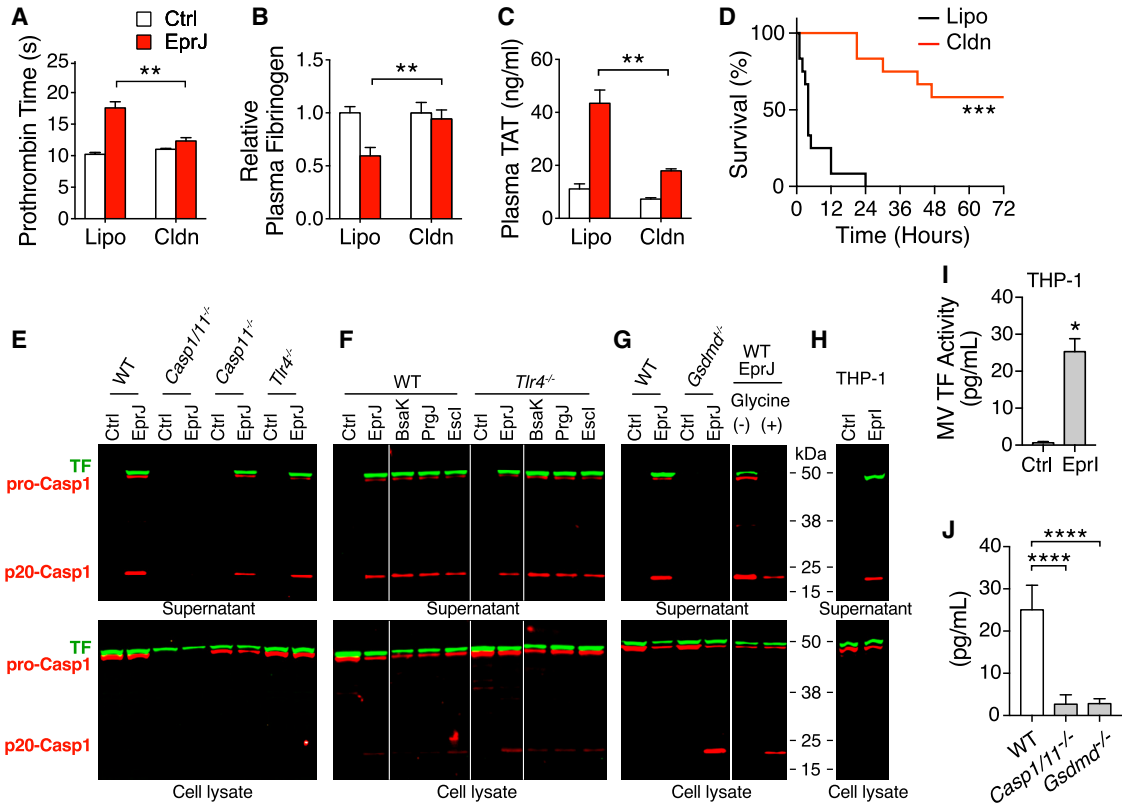

Figure 4. Macrophages Pyroptosis Plays a Critical Role in Inflammasome-Induced Coagulation by Promoting the Release of TF-Positive Microvesicles

(A–C) C57BL/6J mice were injected intravenously with control liposomes (Lipo) or clodronate-containing liposomes (Cldn) 24 h prior to intravenous injection of PBS (Ctrl) or EprJ. Blood was collected 90 min after PBS or EprJ injection. Prothrombin time (A), plasma fibrinogen concentrations (B), and plasma TAT concentrations (C) were measured. Error bars denote SEM; n = 4–6 for all experimental groups. **p < 0.01 (two-way ANOVA with Holm-Sidak multiple comparisons).

(D) C57BL/6J mice were injected intravenously with control liposomes (Lipo) or clodronate-containing liposomes (Cldn) 24 h prior to intravenous injection of a lethal dose EprJ. ***p < 0.01 (log rank [Mantel-Cox] test).

(E) BMDMs from C57BL/6J (WT), Casp1/11-deficient, Casp11-deficient mice, and TLR4-deficient mice were incubated with various T3SS rod proteins (100 ng/mL LFn-rod protein plus 1 μg/mL PA) for 45 min. TF and p20 caspase-1 in the supernatant were detected by fluorescent immunoblot. Cell culture supernatants were precipitated to concentrate protein prior to immunoblot.

(F) BMDMs from C57BL/6J (WT) and TLR4-deficient mice were incubated with various T3SS rod proteins for 45 min. TF and p20 caspase-1 in the supernatant were detected by fluorescent immunoblot.

(G) BMDMs from C57BL/6J (WT) and GSDMD-deficient mice were incubated with EprJ for 45 min. TF and p20 caspase-1 in the supernatant were detected by fluorescent immunoblot. Glycine (+) designates addition of 5 mM glycine as osmoprotectant to prevent pyroptosis-associated membrane rupture.

(H) THP-1 cells were incubated with T3SS needle protein EprI (1 μg/mL LFn-EprI plus 1 μg/mL PA) for 45 min. Cell culture supernatants were precipitated to concentrate protein prior to immunoblot analysis. Data are representative of 3 independent experiments for all the immunoblots (biological replicates).

(I) THP-1 was incubated with EprI for 45 min. MVs were isolated from supernatant, and TF activity was measured. Error bars denote SEM. n = 4–6 for all experimental groups (biological replicates). *p < 0.01 (Student's t test; unpaired).

(J) Plasma MV TF activity. C57BL/6J (WT), Casp1/11-deficient, and GSDMD-deficient mice were injected intravenously with EprJ. Blood were collected 90 min after EprJ injection. MVs were isolated from blood, and TF activity was measured. Error bars denote SEM; n = 4–6 for all experimental groups. ****p < 0.01 (one-way ANOVA with Holm-Sidak multiple comparisons).

See also Figure S5.

Macrophage-Derived TF Is Required for Coagulation Activation following Inflammasome Activation

Monocytes and macrophages are major sources of TF *in vivo* (Pawlinski et al., 2010). Hematopoietic cell-derived TF is a major contributor to the activation of coagulation in mouse models of endotoxemia and sepsis (Franco et al., 2000; Gando et al., 2016; Pawlinski et al., 2010). Macrophages can release TF-positive MVs upon caspase-1 activation by ATP *in vitro* (Rothmeier et al., 2015). As shown in Figure 4E, TF is abundantly expressed in BMDMs as detected by immunoblot. TF is a transmembrane protein present in the cell membrane under resting condition. To determine whether TF is released following inflammasome activation, we incubated mouse BMDMs with EprJ and collected cell culture supernatants. EprJ-challenged, wild-type BMDMs exhibited caspase-1 activation, as revealed by the presence of p20 caspase-1 (Boucher et al., 2018), which was accompanied by TF release into the cell culture supernatants (Figure 4E). EprJ-induced caspase-1 cleavage and TF release were not detected in the BMDMs from *Casp1/11*$^{-/-}$ mice. In contrast, caspase-11 or TLR4 deficiency had no effect on EprJ-induced

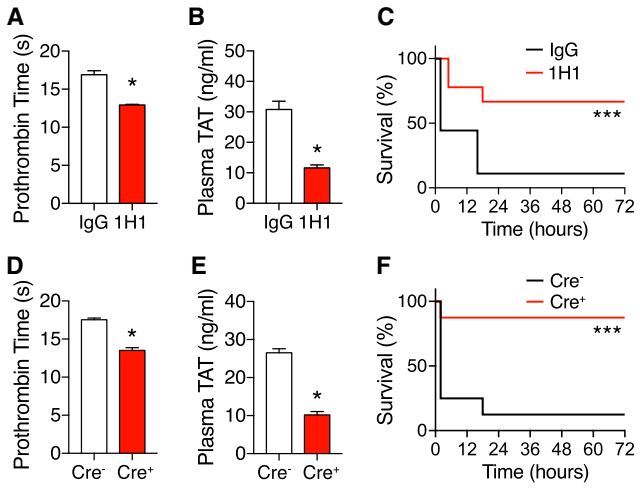

Figure 5. Tissue Factor Inhibition Protects against Inflammasome-Induced Coagulation and Lethality

(A–C) Pharmacological inhibition of TF. C57BL/6J mice were injected intravenously with a rat IgG or a rat anti-mouse TF-neutralizing antibody 1H1 (8 mg/kg). After 2 h, the mice were injected intravenously with EprJ. Blood was collected 90 min after EprJ injection. Prothrombin time (A) and plasma TAT concentrations (B) were measured. Error bars denote SEM; n = 4–5 for all experimental groups. *p < 0.01 (Student's t test; unpaired).

(C) C57BL/6J mice were injected intravenously with a rat IgG or 1H1 (8 mg/kg). After 2 h, the mice were injected intravenously with a lethal dose of EprJ. ***p < 0.01 (log rank [Mantel-Cox] test).

(D–F) Inducible TF-deficient mice were generated by crossing B6.Cg-Tg(UBC-cre/ERT2)1Ejb/J Cre transgenic mice with TF floxed mice. TF-deficient mice or wild-type littermates were injected intravenously with EprJ. Blood was collected 90 min after EprJ injection. Prothrombin time (D) and plasma TAT concentrations (E) were measured. Error bars denote SEM; n = 4–5 for all experimental groups. *p < 0.01 (Student's t test; unpaired).

(F) TF-deficient mice or wild-type littermates were injected with a lethal dose of EprJ. n = 8. ***p < 0.01 (log rank test [Mantel-Cox]).

See also Figure S5.

caspase-1 cleavage and TF release (Figure 4E). These findings demonstrate that TF release from macrophages requires caspase-1-dependent inflammasome activity.

Rod proteins from other bacterial strains, such as *Burkholderia* BsaK, *Salmonella* PrgJ, and *EPEC* EscI, elicited TF release from BMDMs. Consistent with previous reports (Zhao et al., 2011, 2016), all the rod proteins we examined led to caspase-1 activation (Figure S1A) and TF release from both wild-type and TLR4-deficient BMDMs (Figure 4F). T3SS needle proteins can activate the inflammasome in human macrophages (Zhao et al., 2016). *E. coli* T3SS needle protein EprI elicited release of active TF from human-monocyte-like THP-1 cells (Figures 4H and 4I), indicating inflammasome activation may be a conserved mechanism for the initiation of coagulation in both humans and rodents.

We next investigated whether GSDMD-formed pores facilitate the release of TF from macrophages, because TF release elicited by EprJ was abolished in the *Gsdmd*$^{-/-}$ BMDMs (Figure 4G). To prevent pyroptosis-driven cell membrane rupture, we utilized glycine (5 mM) as an osmoprotectant for BMDMs (Fink and Cookson, 2006). Glycine buffering prevented TF release from wild-type cells (Figure 4G), indicating that TF is not released through GSDMD-formed pores, rather rupture of the cell membrane is required for TF release.

Tissue Factor Is Responsible for Inflammasome-Induced Lethality

TF is released from cells in the form of MVs (Grover and Mackman, 2018). In contrast to elevated plasma MV TF activity in EprJ-challenged wild-type mice, both *Casp1/11*$^{-/-}$ and *Gsdmd*$^{-/-}$ mice had significantly lower plasma MV TF activity when challenged with EprJ (Figure 4J), suggesting that GSDMD-dependent pyroptosis promotes the release of TF-positive MVs. Pre-depletion of monocytes and macrophages significantly decreased plasma MV TF activity (Figure S5A), demonstrating that MV TFs released into plasma are mainly from pyroptotic monocytes and macrophages.

To establish the role of TF in pyroptosis-triggered coagulation, we utilized an inhibitory rat anti-mouse TF antibody, 1H1, to block TF activity (Kirchhofer et al., 2005). Mice administered with 1H1, but not a control immunoglobulin G (IgG), were protected from coagulation (Figures 5A and 5B). Mice injected with 1H1 also had improved survival (Figure 5C) after EprJ challenge in comparison to mice administered with a control IgG.

As a complementary approach, we generated a TF-inducible deficient mouse model (because constitutive TF-deficient mice are embryonic lethal). Deletion of TF was controlled by tamoxifen-inducible Cre recombinase expression driven by the human ubiquitin C. Genetic deficiency of TF showed no effect on inflammasome activation and pyroptosis (Figures S5B and S5C) but blocked EprJ-induced coagulation and lethality (Figures 5D–5F). Thus, TF contributes to inflammasome-activation-induced mortality, likely through inducing coagulation.

LPS Induces Coagulation through Noncanonical Inflammasome Pathway

Gram-negative bacteria activate inflammasomes through multiple mechanisms (Hagar et al., 2013; Kayagaki et al., 2013; Miao et al., 2010; Shi et al., 2014; Zanoni et al., 2016; Zhao et al., 2011). LPS is a known activator of inflammasome, although it acts in a noncanonical manner through caspase-11 instead of caspase-1 (Hagar et al., 2013; Kayagaki et al., 2013; Shi et al., 2014; Vanaja et al., 2016; Zanoni et al., 2016). Unlike caspase-1, activation of the caspase-11 pathway requires priming macrophages with toll-like receptor (TLR) ligands or interferons, which induces the expression of multiple components in the noncanonical inflammasome pathway, including caspase-11 (Broz et al., 2012; Case et al., 2013; Rathinam et al., 2012). We determined whether LPS could activate coagulation through the inflammasome activation. Intraperitoneal injection of LPS into wild-type mice primed with polyinosinic:polycytidylic acid (poly(I:C)), a TLR3 agonist, induced a systemic coagulopathy, as demonstrated by prolonged PT (Figure 6A), decreased plasma fibrinogen concentrations (Figure 6B), elevated plasma TAT concentrations (Figure 6C), and decreased total platelet counts (Figure 6D). Blood coagulation was not observed in *Casp11*$^{-/-}$ mice challenged with LPS (Figures 6A–6C), and thrombocytopenia was also attenuated (Figure 6D), suggesting that noncanonical inflammasome activation is required for LPS-elicited coagulation. In contrast, LPS-induced activation of coagulation was independent of TLR4 because *Tlr4*$^{-/-}$ mice responded to LPS to the same extent as wild-type mice in terms of coagulation (Figures 6A–6D). These data are consistent with previous findings that LPS-elicited inflammasome activation is TLR4 independent

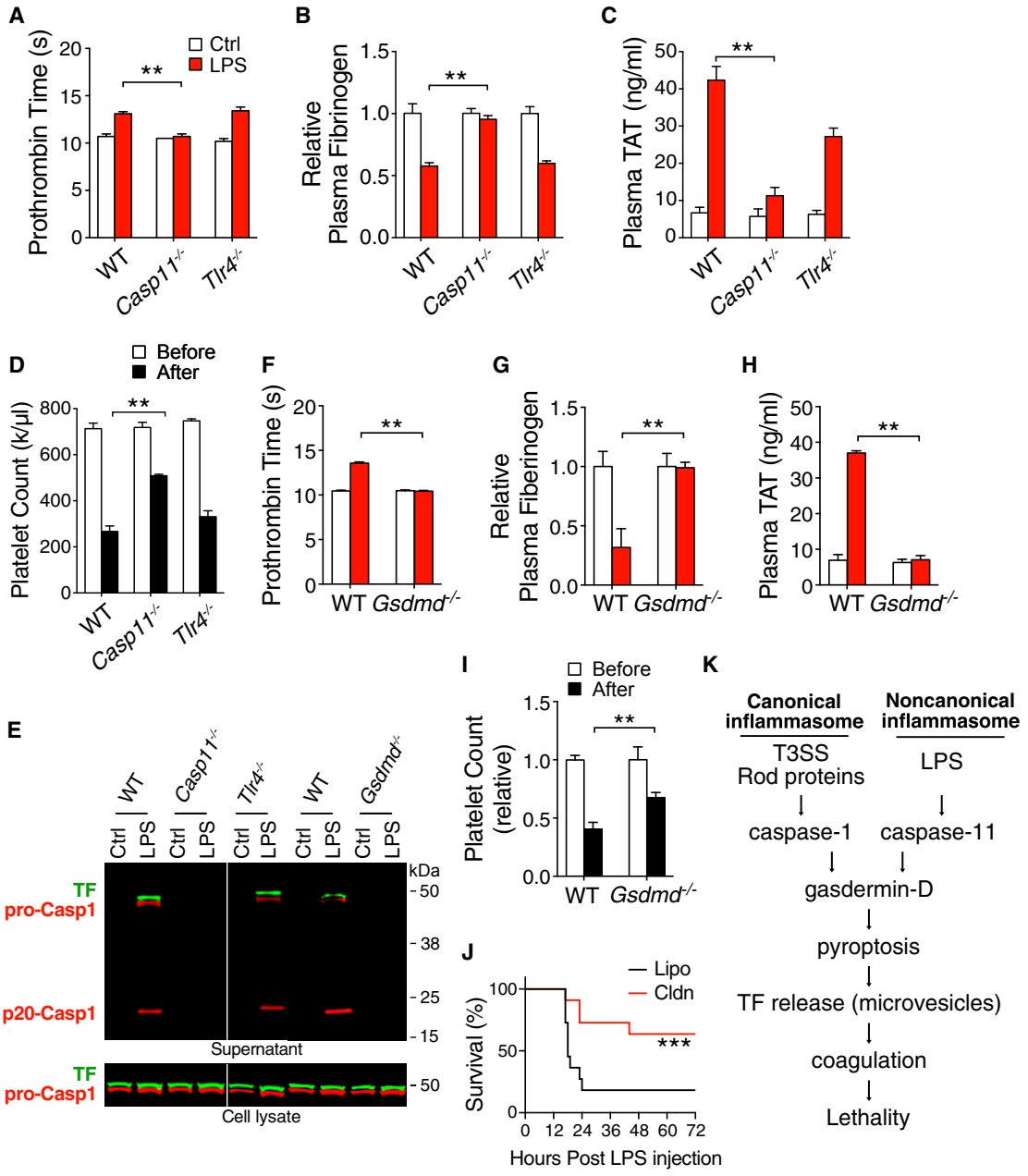

Figure 6. Noncanonical Inflammasome Activation by LPS Triggers Blood Coagulation

(A–D) C57BL/6J mice (WT), Casp11-deficient, and TLR4-deficient mice were injected intraperitoneally with 4 mg/kg poly(I:C) for priming. After 8 h, the mice were injected intraperitoneally with PBS (Ctrl) or 50 mg/kg LPS. Blood was collected 4 h after injection of PBS or LPS injection. Prothrombin time (A), plasma fibrinogen concentrations (B), plasma TAT concentrations (C), and total platelet count before and after LPS injection (D) were measured. Error bars denote SEM; n = 4–6 for all experimental groups. **p < 0.01 (two-way ANOVA with Holm-Sidak multiple comparisons).

(E) BMDMs from C57BL/6J (WT), Casp11-deficient, TLR4-deficient, and GSDMD-deficient mice were incubated with poly(I:C) (1 μg/mL). After 5 h, the cells were transfected with PBS (Ctrl) or LPS (2 μg/mL). Cell culture supernatants were precipitated to concentrate protein prior to immunoblot. Data are representative of 3 independent experiments (biological replicates).

(F–I) C57BL/6J mice (WT) or GSDMD-deficient mice were injected intraperitoneally with 4 mg/kg poly(I:C) for priming. After 8 h, the mice were injected intraperitoneally with PBS (Ctrl) or 50 mg/kg LPS. Blood was collected 4 h after injection of PBS or LPS injection. Prothrombin time (F), plasma fibrinogen concentrations (G), plasma TAT concentrations (H), and total platelet count before and after LPS injection (I) were measured. Error bars denote SEM; n = 4–6 for all experimental groups. **p < 0.01 (two-way ANOVA with Holm-Sidak multiple comparisons).

(J) C57BL/6J mice were injected intravenously with control liposomes (Lipo) or clodronate-containing liposomes (Cldn) 24 h prior to intraperitoneal injection of 4 mg/kg poly(I:C). After 6 h of poly(I:C) injection, the mice were injected with a lethal dose of LPS. ***p < 0.01 (log rank test [Mantel-Cox]).

(K) Model of coagulation triggered by canonical and noncanonical inflammasome activation.

See also Figure S6.

(Hagar et al., 2013; Kayagaki et al., 2013). Transfection of LPS into BMDMs, required to activate inflammasome (Figure S6A), promoted release of TF of BMDMs from wild-type mice and *Tlr4*$^{-/-}$ mice, but not from *Casp11*$^{-/-}$ mice (Figure 6E). Thus, LPS triggers blood coagulation through inflammasome-dependent TF release.

Because LPS elicited coagulation through inflammasome activation, we hypothesize that GSDMD-dependent pyroptosis also drives noncanonical LPS-induced coagulation and lethality using *Gsdmd*$^{-/-}$ mice. Indeed, LPS-induced prolongation of PT (Figure 6F), reduction in plasma fibrinogen concentrations (Figure 6G), and increase in plasma TAT concentrations (Figure 6H) were diminished in *Gsdmd*$^{-/-}$ mice. GSDMD deficiency showed modest but significant protection against LPS-induced thrombocytopenia (Figure 6I).

Two independent groups have reported that lethal sepsis in mice induced by LPS is attributed to caspase-11-dependent pyroptosis (Hagar et al., 2013; Kayagaki et al., 2011). However, it remains unclear which cell types drive lethality. Here, we extended their finding by demonstrating that depletion of monocytes and macrophages significantly decreased plasma MV TF activity (Figure S6B) and improved survival in mice administered a lethal dose of LPS (Figure 6J). Our observations are consistent with those in patients of septic shock, where progression to DIC is associated with increased mortality (Fujishima et al., 2014; Gando et al., 2013; Rangel-Frausto et al., 1995; Venugopal, 2014).

DISCUSSION

Activation of inflammatory caspases is a central mechanism of innate immune response against bacterial infections. However, excessive activation of the inflammatory caspases leads to multiple organ damage and host lethality (Kayagaki et al., 2011; Zhao et al., 2016). Here, we provide a molecular mechanism by which inflammasome activation and pyroptosis cause death of the host. We demonstrate that TF released from pyroptotic macrophages initiates systemic coagulation and thrombosis in tissues, which plays a central role in inflammasome-activation-induced lethality. Identifying DIC as a critical event following inflammasome and pyroptosis opens a direction in studying inflammasome and pyroptosis, as current understanding of the inflammasome function is limited to inflammatory response.

Coagulation induced by EprJ was abolished by caspase-1 or GSDMD deficiency, suggesting that EprJ-induced coagulation activation depends on inflammasome activation and pyroptosis. Because pores formed by GSDMD facilitate the release of the IL-1β and IL-18 (Evavold et al., 2018; He et al., 2015; Monteleone et al., 2018), GSDMD deficiency not only prevents pyroptosis but also diminishes IL-1β and IL-18 secretion. Thus, we utilized mice lacking IL-1β receptor or IL-18 receptor to investigate whether IL-1β and IL-18 contribute to coagulation following inflammasome activation. We found that deficiency of the receptors for IL-1β and IL-18 does not protect against EprJ-elicited coagulation. These data exclude the possibility that inflammasome-activation-induced coagulation requires IL-1β- and IL-18-dependent inflammation, thus establishing pyroptosis as a key event leading to coagulation upon inflammasome activation.

EprJ-induced coagulation is diminished in TF-deficient mice and in mice administered a TF-neutralizing antibody, demonstrating that TF is required for inflammasome-driven coagulation. These findings are consistent with previous studies that TF plays an essential role in sepsis-associated DIC (Franco et al., 2000; Gando et al., 2016; Pawlinski et al., 2004, 2010; Taylor et al., 1991). Our data further show that EprJ-induced lethality was protected by the deficiency of TF or the TF-neutralizing antibody, demonstrating that pyroptosis-induced coagulation is a major cause of host death. Although TF has been recognized as a key initiator of DIC in sepsis, how TF is released to trigger coagulation is largely unknown. We show that MVs isolated from the blood of EprJ-challenged mice have high TF activity, which was abolished by caspase-1 or GSDMD deficiency. Consistent with the *in vivo* data, EprJ treatment increased TF activity in the MVs from BMDMs isolated from wild-type, but not from *Gsdmd*$^{-/-}$ or *Casp1/11*$^{-/-}$ mice. Together, these data suggest that cell membrane fragments of pyroptotic macrophages form TF-positive MVs as a result of thermodynamics. This is consistent with previous findings that caspase-1 activation by ATP promotes TF-positive MV release *in vitro* (Rothmeier et al., 2015). Unlike IL-1β and IL-18, release of TF from macrophages is not through GSDMD pores but requires membrane rupture, suggesting distinct mechanisms are involved. This is not surprising because IL-1β and IL-18 are cytosolic proteins and TF is a transmembrane protein. Besides pyroptosis, necroptosis is another form of lytic programmed cell death (Wallach et al., 2016). Although distinct signaling pathways induce pyroptosis and necroptosis, both forms of cell death lead to ruptured cell membrane, a requirement for TF-positive MV release. Thus, it is likely that necroptosis may also lead to TF release.

Sepsis is a complex process, involving severe inflammation, organ dysfunction, various types of cell death, etc. It is likely that different mechanisms contribute to the development of DIC during sepsis. In this regard, it has been shown that neutrophil extracellular traps (NETs), DNA, and histone play important roles in the development of DIC (Brinkmann and Zychlinsky, 2012; Fuchs et al., 2010; Liaw et al., 2016; McDonald et al., 2017). Inflammasome can be activated by both the pathogen-associated molecular patterns (PAMPs) and the damage-associated molecular patterns (DAMPs). *E. coli*-induced coagulation activation was diminished in the GSDMD-deficient mice, supporting that pyroptosis is at least one of the major mechanisms of DIC in bacterial infection.

Although TF expression in monocytes is enhanced during sepsis or by LPS stimulation (Grover and Mackman, 2018), macrophages express high amounts of TF, which is sufficient to trigger DIC. This conclusion is supported by our data that administration of EprJ or BsaK elicited DIC within 60 min and TF was detected by immunoblot in the cell lysates of macrophages. Consistent with these findings, administration of EprJ-induced clearance of peripheral monocytes within 60 min. Clearance of peripheral monocytes was not due to migration of the cells to tissues, because the total monocytes and macrophages in tissues was also significantly reduced in tissues. Furthermore, we found that administration of EprJ-induced macrophage death in tissues. Thus, administration of EprJ-induced monocytes and macrophage depletion through pyroptosis, and TF released from pyroptotic cells triggered systemic coagulation. Although

administration of clodronate into mice induced monocyte and macrophage depletion through apoptosis to a similar extent as injection of EprJ, clodronate failed to induce DIC and lethality in mice. In contrast, pre-depletion of monocytes and macrophages by clodronate protected against EprJ-elicited DIC and lethality. These data demonstrate that pyroptosis, but not apoptosis, is capable of TF release. Unlike apoptosis, cell death by pyroptosis results in plasma-membrane rupture and the release of cell contents into blood (Jorgensen and Miao, 2015; Wallach et al., 2016), which promotes inflammatory response. Our study identified a function of pyroptosis in triggering coagulation activation through releasing TF.

Although TF is expressed in different cell types (Grover and Mackman, 2018), the major source of TF in blood following inflammasome activation appears to be monocytes and macrophages. These data are consistent with the previous findings that monocytes- and macrophages-derived TF plays an important role in sepsis-associated DIC and also consistent with the findings that pyroptosis mainly occurs in monocytes and macrophages (Jorgensen and Miao, 2015; Wallach et al., 2016). Endothelial cells could undergo pyroptosis upon LPS stimulation (Cheng et al., 2017). However, they express minimal TF, thus unlikely to be a major source of TF in our experimental settings—coagulation was fully activated within 60 min after administration of EprJ, a time frame excluding enhanced TF expression in endothelial cells.

Our data establish inflammasome activation as an important link between inflammation and blood clotting. Specifically, inflammasome activation by bacterial products results in GSDMD-dependent macrophage pyroptosis, leading to the release of TF-positive MVs into the blood, which in turn triggers blood coagulation, resulting in organ damage and lethality. Our findings advance the understanding of the relationship between bacterial infections and coagulation as well as provide evidence that inflammasome may be a potential therapeutic target for sepsis. Our data also suggest that T3SS rod protein-induced coagulation is a robust systemic coagulation model that can be used for developing therapeutics against DIC. Whether similar mechanisms link inflammation to thrombosis in different settings remains to be determined.

STAR★METHODS

Detailed methods are provided in the online version of this paper and include the following:

SUPPLEMENTAL INFORMATION

Supplemental Information can be found online at https://doi.org/10.1016/j.immuni.2019.04.003.

ACKNOWLEDGMENTS

C.W. is supported by AHA Great Rivers Affiliate Postdoctoral Fellowship 16POST31140008 and is a K99 awardee (K99HL145117; NHLBI). J.S. is supported by National Natural Science Foundation of China 81372391. X.L. is supported by NIH R01 GM121796. Y.W. is supported by AHA Great Rivers Affiliate Grant-in-Aid 17GRNT33410327, NSF CHE-1709381, NIH/NIAID R56 AI137020 and R21 AI142063, and NIH/NHLBI R01 HL142640. Z.L. is supported by NIH/NHLBI R01 HL123927 and R01 HL142640. Dr. Wendy Katz provided help with tissue paraffin embedding and sectioning and was supported by NIH/NIGMS Institutional Development Award P20GM103527. Dr. Thomas Wilkop at UK Light Microscopy Core provided help with intravital microscopy. Dr. Wei Li at Marshall University provided help with isolation of mouse cremaster muscle. Dr. Hartmut Weiler at Medical College of Wisconsin and Dr. Rodney M. Camire at the University of Pennsylvania provided fibrin antibodies.

AUTHOR CONTRIBUTIONS

C.W., Y.W., and Z.L. designed and performed the experiments and wrote the manuscript, assisted by W.L., Y.Z., G.Z., X.S., Y.H., S.P.G., X.Z., L.L., B.X., and J.S. X.-A.L., A.D., S.S.S., N.M., and F.S. contributed to manuscript preparation. D.K., T.S., and N.M. provided mice and/or reagents and discussed experiments. All authors discussed the results and commented on the manuscript.

DECLARATION OF INTERESTS

D.K. is an employee of Genentech Inc.

Received: October 26, 2018
Revised: February 4, 2019
Accepted: April 11, 2019
Published: May 7, 2019

REFERENCES

Aglietti, R.A., Estevez, A., Gupta, A., Ramirez, M.G., Liu, P.S., Kayagaki, N., Ciferri, C., Dixit, V.M., and Dueber, E.C. (2016). GsdmD p30 elicited by caspase-11 during pyroptosis forms pores in membranes. Proc. Natl. Acad. Sci. USA *113*, 7858–7863.

Angus, D.C., and van der Poll, T. (2013). Severe sepsis and septic shock. N. Engl. J. Med. *369*, 840–851.

Aziz, M., Jacob, A., Yang, W.L., Matsuda, A., and Wang, P. (2013). Current trends in inflammatory and immunomodulatory mediators in sepsis. J. Leukoc. Biol. *93*, 329–342.

Bach, R., Nemerson, Y., and Konigsberg, W. (1981). Purification and characterization of bovine tissue factor. J. Biol. Chem. *256*, 8324–8331.

Boucher, D., Monteleone, M., Coll, R.C., Chen, K.W., Ross, C.M., Teo, J.L., Gomez, G.A., Holley, C.L., Bierschenk, D., Stacey, K.J., et al. (2018). Caspase-1 self-cleavage is an intrinsic mechanism to terminate inflammasome activity. J. Exp. Med. *215*, 827–840.

Brinkmann, V., and Zychlinsky, A. (2012). Neutrophil extracellular traps: is immunity the second function of chromatin? J. Cell Biol. *198*, 773–783.

Broz, P., Ruby, T., Belhocine, K., Bouley, D.M., Kayagaki, N., Dixit, V.M., and Monack, D.M. (2012). Caspase-11 increases susceptibility to Salmonella infection in the absence of caspase-1. Nature *490*, 288–291.

Case, C.L., Kohler, L.J., Lima, J.B., Strowig, T., de Zoete, M.R., Flavell, R.A., Zamboni, D.S., and Roy, C.R. (2013). Caspase-11 stimulates rapid flagellin-independent pyroptosis in response to Legionella pneumophila. Proc. Natl. Acad. Sci. USA *110*, 1851–1856.

Cheng, K.T., Xiong, S., Ye, Z., Hong, Z., Di, A., Tsang, K.M., Gao, X., An, S., Mittal, M., Vogel, S.M., et al. (2017). Caspase-11-mediated endothelial pyroptosis underlies endotoxemia-induced lung injury. J. Clin. Invest. *127*, 4124–4135.

Ding, J., Wang, K., Liu, W., She, Y., Sun, Q., Shi, J., Sun, H., Wang, D.C., and Shao, F. (2016). Pore-forming activity and structural autoinhibition of the gasdermin family. Nature *535*, 111–116.

Effenberger-Neidnicht, K., and Hartmann, M. (2018). Mechanisms of hemolysis during sepsis. Inflammation *41*, 1569–1581.

Evavold, C.L., Ruan, J., Tan, Y., Xia, S., Wu, H., and Kagan, J.C. (2018). The pore-forming protein gasdermin D regulates interleukin-1 secretion from living macrophages. Immunity *48*, 35–44.e6.

Fink, S.L., and Cookson, B.T. (2006). Caspase-1-dependent pore formation during pyroptosis leads to osmotic lysis of infected host macrophages. Cell. Microbiol. *8*, 1812–1825.

Franco, R.F., de Jonge, E., Dekkers, P.E.P., Timmerman, J.J., Spek, C.A., van Deventer, S.J.H., van Deursen, P., van Kerkhoff, L., van Gemen, B., ten Cate, H., et al. (2000). The in vivo kinetics of tissue factor messenger RNA expression during human endotoxemia: relationship with activation of coagulation. Blood *96*, 554–559.

Fuchs, T.A., Brill, A., Duerschmied, D., Schatzberg, D., Monestier, M., Myers, D.D., Jr., Wrobleski, S.K., Wakefield, T.W., Hartwig, J.H., and Wagner, D.D. (2010). Extracellular DNA traps promote thrombosis. Proc. Natl. Acad. Sci. USA *107*, 15880–15885.

Fujii, T., Tamura, M., Tanaka, S., Kato, Y., Yamamoto, H., Mizushina, Y., and Shiroishi, T. (2008). Gasdermin D (Gsdmd) is dispensable for mouse intestinal epithelium development. Genesis *46*, 418–423.

Fujishima, S., Gando, S., Saitoh, D., Mayumi, T., Kushimoto, S., Shiraishi, S., Ogura, H., Takuma, K., Kotani, J., Ikeda, H., et al.; Japanese Association for Acute Medicine Sepsis Registry (JAAM SR) Study Group (2014). A multicenter, prospective evaluation of quality of care and mortality in Japan based on the Surviving Sepsis Campaign guidelines. J. Infect. Chemother. *20*, 115–120.

Gando, S., Levi, M., and Toh, C.H. (2016). Disseminated intravascular coagulation. Nat. Rev. Dis. Primers *2*, 16037.

Gando, S., Saitoh, D., Ogura, H., Fujishima, S., Mayumi, T., Araki, T., Ikeda, H., Kotani, J., Kushimoto, S., Miki, Y., et al.; Japanese Association for Acute Medicine Sepsis Registry Study Group (2013). A multicenter, prospective validation study of the Japanese Association for Acute Medicine disseminated intravascular coagulation scoring system in patients with severe sepsis. Crit. Care *17*, R111.

Grover, S.P., and Mackman, N. (2018). Tissue factor: an essential mediator of hemostasis and trigger of thrombosis. Arterioscler. Thromb. Vasc. Biol. *38*, 709–725.

Hagar, J.A., Powell, D.A., Aachoui, Y., Ernst, R.K., and Miao, E.A. (2013). Cytoplasmic LPS activates caspase-11: implications in TLR4-independent endotoxic shock. Science *341*, 1250–1253.

He, W.T., Wan, H., Hu, L., Chen, P., Wang, X., Huang, Z., Yang, Z.H., Zhong, C.Q., and Han, J. (2015). Gasdermin D is an executor of pyroptosis and required for interleukin-1β secretion. Cell Res. *25*, 1285–1298.

Hui, K.Y., Haber, E., and Matsueda, G.R. (1983). Monoclonal antibodies to a synthetic fibrin-like peptide bind to human fibrin but not fibrinogen. Science *222*, 1129–1132.

Ivanciu, L., Toso, R., Margaritis, P., Pavani, G., Kim, H., Schlachterman, A., Liu, J.H., Clerin, V., Pittman, D.D., Rose-Miranda, R., et al. (2011). A zymogen-like factor Xa variant corrects the coagulation defect in hemophilia. Nat. Biotechnol. *29*, 1028–1033.

Jorgensen, I., and Miao, E.A. (2015). Pyroptotic cell death defends against intracellular pathogens. Immunol. Rev. *265*, 130–142.

Kayagaki, N., Stowe, I.B., Lee, B.L., O'Rourke, K., Anderson, K., Warming, S., Cuellar, T., Haley, B., Roose-Girma, M., Phung, Q.T., et al. (2015). Caspase-11 cleaves gasdermin D for non-canonical inflammasome signalling. Nature *526*, 666–671.

Kayagaki, N., Warming, S., Lamkanfi, M., Vande Walle, L., Louie, S., Dong, J., Newton, K., Qu, Y., Liu, J., Heldens, S., et al. (2011). Non-canonical inflammasome activation targets caspase-11. Nature *479*, 117–121.

Kayagaki, N., Wong, M.T., Stowe, I.B., Ramani, S.R., Gonzalez, L.C., Akashi-Takamura, S., Miyake, K., Zhang, J., Lee, W.P., Muszyński, A., et al. (2013). Noncanonical inflammasome activation by intracellular LPS independent of TLR4. Science *341*, 1246–1249.

Kirchhofer, D., Moran, P., Bullens, S., Peale, F., and Bunting, S. (2005). A monoclonal antibody that inhibits mouse tissue factor function. J. Thromb. Haemost. *3*, 1098–1099.

Lamkanfi, M., and Dixit, V.M. (2014). Mechanisms and functions of inflammasomes. Cell *157*, 1013–1022.

Latz, E., Xiao, T.S., and Stutz, A. (2013). Activation and regulation of the inflammasomes. Nat. Rev. Immunol. *13*, 397–411.

Levi, M., and Ten Cate, H. (1999). Disseminated intravascular coagulation. N. Engl. J. Med. *341*, 586–592.

Levi, M., ten Cate, H., Bauer, K.A., van der Poll, T., Edgington, T.S., Büller, H.R., van Deventer, S.J., Hack, C.E., ten Cate, J.W., and Rosenberg, R.D. (1994). Inhibition of endotoxin-induced activation of coagulation and fibrinolysis by pentoxifylline or by a monoclonal anti-tissue factor antibody in chimpanzees. J. Clin. Invest. *93*, 114–120.

Liaw, P.C., Ito, T., Iba, T., Thachil, J., and Zeerleder, S. (2016). DAMP and DIC: the role of extracellular DNA and DNA-binding proteins in the pathogenesis of DIC. Blood Rev. *30*, 257–261.

Liu, X., Zhang, Z., Ruan, J., Pan, Y., Magupalli, V.G., Wu, H., and Lieberman, J. (2016). Inflammasome-activated gasdermin D causes pyroptosis by forming membrane pores. Nature *535*, 153–158.

McDonald, B., Davis, R.P., Kim, S.J., Tse, M., Esmon, C.T., Kolaczkowska, E., and Jenne, C.N. (2017). Platelets and neutrophil extracellular traps collaborate to promote intravascular coagulation during sepsis in mice. Blood *129*, 1357–1367.

Miao, E.A., Mao, D.P., Yudkovsky, N., Bonneau, R., Lorang, C.G., Warren, S.E., Leaf, I.A., and Aderem, A. (2010). Innate immune detection of the type III secretion apparatus through the NLRC4 inflammasome. Proc. Natl. Acad. Sci. USA *107*, 3076–3080.

Milne, J.C., Blanke, S.R., Hanna, P.C., and Collier, R.J. (1995). Protective antigen-binding domain of anthrax lethal factor mediates translocation of a heterologous protein fused to its amino- or carboxy-terminus. Mol. Microbiol. *15*, 661–666.

Monteleone, M., Stanley, A.C., Chen, K.W., Brown, D.L., Bezbradica, J.S., von Pein, J.B., Holley, C.L., Boucher, D., Shakespear, M.R., Kapetanovic, R., et al. (2018). Interleukin-1β maturation triggers its relocation to the plasma membrane for gasdermin-D-gependent and -independent secretion. Cell Rep. *24*, 1425–1433.

Morrissey, J.H., Fakhrai, H., and Edgington, T.S. (1987). Molecular cloning of the cDNA for tissue factor, the cellular receptor for the initiation of the coagulation protease cascade. Cell *50*, 129–135.

Neyman, M., Gewirtz, J., and Poncz, M. (2008). Analysis of the spatial and temporal characteristics of platelet-delivered factor VIII-based clots. Blood *112*, 1101–1108.

Parise, L.V., Venton, D.L., and Le Breton, G.C. (1984). Arachidonic acid-induced platelet aggregation is mediated by a thromboxane A2/prostaglandin H2 receptor interaction. J. Pharmacol. Exp. Ther. *228*, 240–244.

Pawlinski, R., Pedersen, B., Erlich, J., and Mackman, N. (2004). Role of tissue factor in haemostasis, thrombosis, angiogenesis and inflammation: lessons from low tissue factor mice. Thromb. Haemost. *92*, 444–450.

Pawlinski, R., Wang, J.G., Owens, A.P., 3rd, Williams, J., Antoniak, S., Tencati, M., Luther, T., Rowley, J.W., Low, E.N., Weyrich, A.S., and Mackman, N. (2010). Hematopoietic and nonhematopoietic cell tissue factor activates the coagulation cascade in endotoxemic mice. Blood *116*, 806–814.

Rangel-Frausto, M.S., Pittet, D., Costigan, M., Hwang, T., Davis, C.S., and Wenzel, R.P. (1995). The natural history of the systemic inflammatory response syndrome (SIRS). A prospective study. JAMA *273*, 117–123.

Rathinam, V.A., Vanaja, S.K., Waggoner, L., Sokolovska, A., Becker, C., Stuart, L.M., Leong, J.M., and Fitzgerald, K.A. (2012). TRIF licenses caspase-11-dependent NLRP3 inflammasome activation by gram-negative bacteria. Cell *150*, 606–619.

Rothmeier, A.S., Marchese, P., Petrich, B.G., Furlan-Freguia, C., Ginsberg, M.H., Ruggeri, Z.M., and Ruf, W. (2015). Caspase-1-mediated pathway promotes generation of thromboinflammatory microparticles. J. Clin. Invest. *125*, 1471–1484.

Ruan, J., Xia, S., Liu, X., Lieberman, J., and Wu, H. (2018). Cryo-EM structure of the gasdermin A3 membrane pore. Nature *557*, 62–67.

Sborgi, L., Rühl, S., Mulvihill, E., Pipercevic, J., Heilig, R., Stahlberg, H., Farady, C.J., Müller, D.J., Broz, P., and Hiller, S. (2016). GSDMD membrane pore formation constitutes the mechanism of pyroptotic cell death. EMBO J. *35*, 1766–1778.

Schroder, K., and Tschopp, J. (2010). The inflammasomes. Cell *140*, 821–832.

Shi, J., Zhao, Y., Wang, K., Shi, X., Wang, Y., Huang, H., Zhuang, Y., Cai, T., Wang, F., and Shao, F. (2015). Cleavage of GSDMD by inflammatory caspases determines pyroptotic cell death. Nature *526*, 660–665.

Shi, J., Zhao, Y., Wang, Y., Gao, W., Ding, J., Li, P., Hu, L., and Shao, F. (2014). Inflammatory caspases are innate immune receptors for intracellular LPS. Nature *514*, 187–192.

Taylor, F.B., Jr., Chang, A., Ruf, W., Morrissey, J.H., Hinshaw, L., Catlett, R., Blick, K., and Edgington, T.S. (1991). Lethal E. coli septic shock is prevented by blocking tissue factor with monoclonal antibody. Circ. Shock *33*, 127–134.

Vanaja, S.K., Russo, A.J., Behl, B., Banerjee, I., Yankova, M., Deshmukh, S.D., and Rathinam, V.A.K. (2016). Bacterial outer membrane vesicles mediate cytosolic localization of LPS and caspase-11 activation. Cell *165*, 1106–1119.

Venugopal, A. (2014). Disseminated intravascular coagulation. Indian J. Anaesth. *58*, 603–608.

von Moltke, J., Trinidad, N.J., Moayeri, M., Kintzer, A.F., Wang, S.B., van Rooijen, N., Brown, C.R., Krantz, B.A., Leppla, S.H., Gronert, K., and Vance, R.E. (2012). Rapid induction of inflammatory lipid mediators by the inflammasome in vivo. Nature *490*, 107–111.

Wada, H., Matsumoto, T., and Yamashita, Y. (2014). Diagnosis and treatment of disseminated intravascular coagulation (DIC) according to four DIC guidelines. J. Intensive Care *2*, 15.

Wallach, D., Kang, T.B., Dillon, C.P., and Green, D.R. (2016). Programmed necrosis in inflammation: toward identification of the effector molecules. Science *352*, aaf2154.

Weiler-Guettler, H., Christie, P.D., Beeler, D.L., Healy, A.M., Hancock, W.W., Rayburn, H., Edelberg, J.M., and Rosenberg, R.D. (1998). A targeted point mutation in thrombomodulin generates viable mice with a prethrombotic state. J. Clin. Invest. *101*, 1983–1991.

Xiang, B., Zhang, G., Guo, L., Li, X.A., Morris, A.J., Daugherty, A., Whiteheart, S.W., Smyth, S.S., and Li, Z. (2013). Platelets protect from septic shock by inhibiting macrophage-dependent inflammation via the cyclooxygenase 1 signalling pathway. Nat. Commun. *4*, 2657.

Zanoni, I., Tan, Y., Di Gioia, M., Broggi, A., Ruan, J., Shi, J., Donado, C.A., Shao, F., Wu, H., Springstead, J.R., and Kagan, J.C. (2016). An endogenous caspase-11 ligand elicits interleukin-1 release from living dendritic cells. Science *352*, 1232–1236.

Zhao, Y., Shi, J., Shi, X., Wang, Y., Wang, F., and Shao, F. (2016). Genetic functions of the NAIP family of inflammasome receptors for bacterial ligands in mice. J. Exp. Med. *213*, 647–656.

Zhao, Y., Yang, J., Shi, J., Gong, Y.N., Lu, Q., Xu, H., Liu, L., and Shao, F. (2011). The NLRC4 inflammasome receptors for bacterial flagellin and type III secretion apparatus. Nature *477*, 596–600.

STAR★METHODS

KEY RESOURCES TABLE

REAGENT or RESOURCE	SOURCE	IDENTIFIER
Antibodies		
1H1 anti-TF antibody	Genentech	Kirchhofer et al., 2005
HTF-1 anti-TF antibody	BD Biosciences	Cat# 550252; RRID: AB_393557
Anti-TF antibody (for Western)	Abcam	Cat# ab151748
Anti-caspase-1 (p20) (mouse)	Adipogen	Cat# AG-20B-0042-C100; RRID: AB_2755041
Anti-caspase-1(p20) (human)	Adipogen	Cat# AG-20B-0048-C100; RRID: AB_2490257
Anti-fibrin antibody 59D8	Medical College of Wisconsin, University of Pennsylvania	Hui et al., 1983
Anti-IL1β	GeneTex	Cat# GTX74034
Anti-fibrinogen	Dako	Cat# A0080
Anti-β-Actin	Biorad antibodies	Cat# MCA5775GA
Anti-CD115-Alexa 488, clone AFS98	eBioscience	Cat# 53-1152-81
Anti-CD45-APC-Cy7, clone 30-F11	BD Biosciences	Cat# 557659
anti-F4/80-APC, clone C1:A3-1	Biorad antibody	Cat# MCA497APC
Biotinylated goat anti-mouse IgG	Vector	Cat# BA-9200
IRDye® 680RD Goat anti-Mouse IgG (H + L)	LI-COR	Cat# 925-68070
IRDye® 800CW Goat anti-Rabbit IgG (H + L)	LI-COR	Cat# 925-32211
Bacterial and Virus Strains		
E.coli	ATCC	Cat# 49106
Chemicals, Peptides, and Recombinant Proteins		
PA	Z.L. laboratory	Zhao et al., 2011
LFn-EprJ	Z.L. laboratory	This paper
LPS (*E. coli* O111:B4)	Sigma	Cat# L4130
Poly(I:C)	Invivogen	Cat# tlrl-picw
Tamoxifen	Sigma	Cat# T5648
FuGENE HD	Promega	Cat# E2311
Opti-MEM	Life Technologies	Cat# 31985-070
Clodronate liposome kit	Encapsula NanoSciences	Cat# CLD-8909
HisPur Ni-NTA resin	ThermoFisher	Cat# 88222
T-PER tissue protein extraction	ThermoFisher	Cat# 78510
Cocktail inhibitor	Sigma	Cat# P8340
Alexa Fluor 568 Antibody Labeling Kit	ThermoFisher	Cat# A20184
Critical Commercial Assays		
Thromboplastin-D	Pacific Hemostasis	Cat# 100357
TAT ELISA kit	Abcam	Cat# ab137994
CellTiter-Glo Luminescent Cell Viability Assay	Promega	Cat# G7571
CytoTox 96 Non-Radioactive Cytotoxicity Assay	Promega	Cat# G1780
Experimental Models: Cell Lines		
Mouse Primary Bone Marrow Derived Macrophages	Z.L. laboratory	This paper
THP-1	ATCC	Cat# TIB-202

(*Continued on next page*)

Continued

REAGENT or RESOURCE	SOURCE	IDENTIFIER
Experimental Models: Organisms/Strains		
C57BL/6J	The Jackson Laboratory	JAX: 000664
Casp1/11$^{-/-}$	The Jackson Laboratory	JAX: 016621
Casp1$^{-/-}$	Genentech Inc	Kayagaki et al., 2015
Casp11$^{-/-}$	The Jackson Laboratory	JAX: 024698
Tlr4$^{-/-}$	The Jackson Laboratory	JAX: 007227
Gsdmd$^{-/-}$	National Institute of Genetics, Japan	Fujii et al., 2008
Il1r$^{-/-}$	The Jackson Laboratory	JAX: 003245
Il18r$^{-/-}$	The Jackson Laboratory	JAX: 004131
B6.Cg-Tg(UBC-cre/ERT2)1Ejb/J	The Jackson Laboratory	JAX: 007001
C57BL/6-Tg(CAG-EGFP)1Osb/J	The Jackson Laboratory	JAX: 003291
F3$^{fl/fl}$	Mackman Laboratory	RRID: IMSR_; JAX: 028721
Software and Algorithms		
FlowJo v10.07 (mac)	FLOWJO	N/A
GraphPad Prism 7 (mac)	GraphPad	N/A

CONTACT FOR REAGENT AND RESOURCE SHARING

Further information and requests for resources and reagents should be directed to and will be fulfilled by the Lead Contact, Zhenyu Li (zhenyuli08@uky.edu).

EXPERIMENTAL MODEL AND SUBJECT DETAILS

Mice

Wild-type C57BL/6J, *Casp1/11*$^{-/-}$, *Casp1*$^{-/-}$, *Casp11*$^{-/-}$, *Tlr4*$^{-/-}$, *Gsdmd*$^{-/-}$, B6.Cg-Tg(UBC-cre/ERT2)1Ejb/J Cre transgenic mice, and TF floxed mice were housed in the University of Kentucky Animal Care Facility, following institutional and National Institutes of Health guidelines after approval by the Institutional Animal Care and Use Committee. *Il1r*$^{-/-}$ mice and *Il18r*$^{-/-}$ mice were housed in the Animal Care Facility at National Institute of Biological Sciences, following the Ministry of Health national guidelines for housing and care of laboratory animals and performed in accordance with institutional regulations after review and approval by the Institutional Animal Care and Use Committee. Male mice at 8-12 weeks were used in all experiments.

In vivo Challenges

For EprJ challenge, purified PA and LFn-EprJ in PBS were administered via retro-orbital injection. For LPS challenge, mice were given poly(I:C) obtained from Invivogen at 4 mg/kg by intraperitoneal injection for priming. After 8 hours of priming, mice were injected intraperitoneally with LPS from *E. coli* O111:B4 (Sigma, Cat#L4130).

Intravital Microscopy of Cremaster Vasculature

Mice were anaesthetized with Avertin and fixed on a custom built-stage to maintain a physiological temperature. Then the animals were injected (retro-orbital) with washed GFP-platelets (2.5×10^8) isolated from the C57BL/6-Tg(CAG-EGFP)1Osb/J mice and Alexa568-labeled fibrin antibody 59D8 (0.15 mg/kg) along with EprJ. Cremaster muscle was isolated immediately after injection. Images were acquired at the same locations 15 min and 60 min after injection on Zeiss LSM880 with 10X Zeiss W Plan-Apochromat under fast Airyscan mode (419x419 μm at 3.6 frames per second). Image and videos were processed in Imaris x64 9.2.0.

Pharmacological and Genetic TF Inhibition

Pharmacological approach: Rat IgG (Sigma) or 1H1 anti-TF antibody (Genentech) at 8 mg/kg was given via retro-orbital injection 2 hours prior to PBS or EprJ injection. Genetic approach: B6.Cg-Tg(UBC-cre/ERT2)1Ejb/J Cre transgenic mice were crossed with TF floxed mice ($F3^{fl/fl}$) to generate inducible TF deficient mice, $F3^{fl/fl}$-ER^{T2+}. $CreER^{T2}$-recombinase expression for removal of TF was induced by intraperitoneal injections of tamoxifen (Sigma) at 100 mg/kg per day for 5 consecutive days at 4 to 5 weeks of age, and subsequent experiments were carried out at 5 weeks post-induction.

BMDM Cultures

BMDMs were isolated and seeded into 12-well cell culture plate at a density of 1×10^6 cells/well in 1 mL of RPMI-1640 medium containing 15% L929-cell conditioned medium (LCM). BMDMs were allowed to settle overnight and refreshed with 1 mL of Opti-MEM (Life Technologies, Cat#31985-070) before purified protein were added (EprJ at 100 ng/ml and PA at 1 μg/ml). For study of LPS,

BMDMs were primed for 5 h with 1 μg/ml poly(I:C), then transfected with 2 μg/ml LPS using FuGENE HD (Promega, Cat#E2311). In brief, a mixture of 2 μL of LPS (1 mg/m) and 3 μL of FuGENE HD reagent was incubated for 5 minutes at room temperature then added to the 12-well plate.

THP-1 Culture

THP-1 cells were obtained from ATCC and cultured in RPMI1640 containing 10% FBS. Macrophage differentiation was induced by incubating THP-1 cells with PMA at 5 ng/ml for 48 hours.

Monocytes and Macrophages Depletion

Mice were administered clodronate liposome at 40 mg/kg or control liposome (Encapsula NanoSciences, Nashville, TN) via retro-orbital injection 24 hours before EprJ or LPS challenge.

METHOD DETAILS

LFn Fusion Protein Purification

Protein expression was induced in *E. coli* BL21 strains at 37°C for 4 hours with 0.5 mM IPTG after OD_{600} reached 0.8-0.9. Bacteria were collected and lysed in 50 mM Tris-HCL and 300 mM NaCl. Proteins containing a His-tag were purified by affinity chromatography using HisPur Ni-NTA resin (Thermo scientific, Cat#88222). To minimize endotoxin contamination, 60% isopropanol was added to the wash buffer. Proteins were then eluted with 250 mM imidazole in 50 mM Tris-HCL and 300 mM NaCl, and subsequently dialyzed against PBS to remove imidazole. Protein concentrations were estimated against BSA standards on SDS-PAGE gels after Coomassie blue staining.

Prothrombin Time (PT)

Blood were collected from tribromoethanol (Avertin)-anaesthetized mice by cardiac puncture with a 23-gauge needle attached to a syringe pre-filled with 3.8% trisodium citrate as anticoagulant (final ratio at 1:10). Blood were centrifuged at 1,500 g for 15 minutes at 4°C to obtain plasma. Prothrombin time (PT) was determined with Thromboplastin-D (Pacific Hemostasis, Cat#100357/lot965299) in a manual setting according to manufacturer's instruction, using CHRONO-LOG #367 plastic cuvette.

Plasma TAT Concentrations

Plasma TAT concentrations were determined using a mouse TAT ELISA kit (Abcam, Cat#ab137994) at 1:50 dilution according to manufacturer's instruction. Plasma were collected as mentioned above in PT.

Total Platelet Counts

Blood were collected via retro-orbital bleeding into tubes containing EDTA. Total platelet counts were acquired on HEMAVET 950 (Drew Scientific) or ProCyte DX Hematology Analyzer (IDEXX Laboratories, Inc.).

Tissue Preparation and Immunohistochemistry

Mice were perfused via both right and left ventricles with PBS and then perfusion-fixed with 10% formalin under physiological pressure for 30-45 minutes. Tissues were collected and embedded in paraffin, then sectioned serially at 5 μm. Anti-fibrin antibody 59D8 (kindly provided by Dr. Hartmut Weiler at Medical College of Wisconsin and Dr. Rodney M. Camire at the University of Pennsylvania) at 4 μg/ml was used for staining fibrin deposition, with biotinylated goat anti-mouse IgG (Vector, Cat#BA-9200) at 1:200 dilution as secondary antibody for developing positive staining.

Glycine as Osmoprotectant

Glycine (5 mM) was added to the cell culture media 30 min before EprJ stimulation to prevent pyroptosis-associated cell membrane rupture.

Fibrin Extraction for Immunoblot

Frozen tissues were homogenized in 10 volumes (mg: μl) of T-PER tissue protein extraction reagent (Thermo#78510) containing cocktail inhibitor (Sigma#P8340) and PMSF. After centrifugation at 10,000 g for 10 min, supernatant was collected for β actin detection. Pellet was homogenized in 3 M urea and vortexed for 2 hr at 37°C. After centrifugation at 14,000 g for 15 min, pellet was suspended in immunoblot sample buffer (reducing) and vortexed at 65°C for 30 min and ready for fibrin detection.

Fluorescent Immunoblot

For detection of active caspase-1 and TF by immunoblot, cells were washed with cold PBS and lysed with SDS sample buffer. Culture supernatants were precipitated with 1/10 volume of 2% sodium cholate and 1/10 volume of 100% trichloroacetic acid (TCA), and then dissolved in SDS sample buffer. Total protein from lysates and supernatants (equivalent to 5 $x10^4$ cells) was analyzed by fluorescent Immunoblot for multiplex detection. TF was detected using anti-tissue factor (Abcam, Cat#ab151748, rabbit monoclonal) at 1:1000 dilution. Both pro-caspase-1 and p20 caspase-1 were determined using anti-caspase-1(p20)

(Adipogen, Cat#AG-20B-0042-C100 for mouse BMDMs, AG-20B-0048-C100 for THP-1 cells) at 1:1000 dilution. IL-1β (p17) was detected using anti-IL-1β (GeneTex Cat#GTX74034). Tissue factor and caspase-1 were visualized on the same blot in the 800 nm (IRDye 800CW) and 700 nm (IRDye 680RD) channel, respectively, with LI-COR Odyssey Classic Imager. Plasma fibrinogen (equivalent to 0.03 μL of plasma) was detected using anti-fibrinogen (Dako Cat#A0080, rabbit polyclonal) at 1:3000 dilution, and imaged in the 800 nm (IRDye 800CW) channel. Tissue fibrin was detected using anti-fibrin (59D8) at 1 μg/ml and imaged in the 700 nm (IRDye 680RD) channel.

Isolation of MVs from Mouse Plasma

Plasma was collected as mentioned above in PT. Then 50 μL of mouse plasma was diluted with 1 mL of HBSA (137 mM NaCl, 5.38 mM KCl, 5.55 mM glucose, 10 mM HEPES, 0.1% bovine serum albumin, pH 7.5). MVs were pelleted at 20,000 g for 20 min at 4°C, washed once with 1 mL of HBSA and re-suspended in 100 μL HBSA.

Isolation of MVs from Cell Culture Supernatant

Cell debris were removed from cell culture supernatant by centrifugation at 2600 x g for 5 min. MVs were then pelleted at 20,000 g for 20 min at 4°C, resuspended in PBS.

MV TF Activity Assay

Samples (50 μL each) were incubated with the 1H1 anti-TF antibody at 100 μg/ml (Genentech) for murine samples, HTF-1 anti-TF antibody at 8 μg/ml (BD Bioscience) for human samples or respective IgG controls for 15 min at room temperature. Next, 50 μL of HBSA containing 10 nM mouse FVIIa (Enzyme Research Laboratories, South Bend, IN), 300 nM human FX (Enzyme Research Laboratories) and 10 mM $CaCl_2$ were added to the sample and incubated for 2 hours at 37°C in a 96-well plate. FXa generation was stopped by the addition of 25 μL of 25 mM EDTA buffer. Finally, 25 μL of the chromogenic substrate Pefachrome FXa 8595 (4 mM, Pentapharm, Switzerland) was added and the mixture incubated at 37°C for 15 min. Absorbance at 405 nm was measured using a Spectramax microplate reader (Molecular Devices, San Jose, CA). The procoagulant activity (PCA) of the sample was calculated by reference to a standard curve generated using recombinant human relipidated TF (0– 55 pg/ml, Siemens, Munich, Germany). The TF-dependent PCA generation (pg/ml) was determined by subtracting the amount of PCA generated in the presence of blocking antibodies from the amount of total PCA generated in the presence of the IgG controls.

Cell Viability

BMDMs cell viability was determined using CellTiter-Glo Luminescent Cell Viability Assay (Promega, Cat#G7571). Briefly, 100 μL of assay buffer was added to each well containing 100 μL cell culture (1 $x10^5$ cells) in a 96-well plate. After incubation for 5-10 minutes, luminescence was recorded as an indicator of ATP concentrations in metabolically active cells.

Cytotoxicity

BMDMs cell cytotoxicity, as LDH concentration in cell culture supernatant, was determined using CytoTox 96 Non-Radioactive Cytotoxicity Assay (Promega, Cat#G1780) according to manufacturer's instruction.

Flow Cytometry

Anti-CD115-Alexa 488, clone AFS98 (eBioscience, Cat#53-1152-81); anti-CD45-APC-Cy7, clone 30-F11 (BD Biosciences, Cat#557659); and anti-F4/80-APC, clone C1:A3-1, (Biorad antibody, Cat#MCA497APC) were used for flow cytometric analysis in the study. Monocytes were identified as CD45+CD115- in blood and CD45+CD115+F4/80- in lung and spleen. Macrophages were identified as CD45+F4/80+. Data were acquired on an LSRII (BD Biosciences) and analyzed with FlowJo v10.07. To obtain single cell suspension, tissues were digested with a cocktail of 1 mg/ml collagenase A (Sigma, Cat#0103586001) and 100 ug/ml DNase I (Sigma, Cat#1010415900s1) in PBS at 37°C for 30 minutes.

QUANTIFICATION AND STATISTICAL ANALYSIS

Data are represented as mean ± SEM. Student's t test (two-sided) was used to compare two-group data with normal distribution and equivalent variance; for multiple-group with two independent factors, two-way ANOVA with Holm-Sidak multiple comparisons was used for normally distributed variables. $p < 0.05$ was considered statistically significant. All statistical analyses were conducted on biological replicates in GraphPad Prism 7.

Platelets were GFP positive (isolated from C57BL/6-Tg(CAG-EGFP)1Osb/J mice) and fibrin were detected with Alexa568-labeled fibrin antibody 59D8. Time series images were acquired at the same location of cremaster vasculature, 15 min and 60 min after EprJ injection, on Zeiss LSM880 with 10X Zeiss W Plan-Apochromat under fast Airyscan mode (419×419 μm at 3.6 frames per second). Image and videos were processed in Imaris x64 9.2.0.